Evaluation of absolute charge density at the bottom of high aspect capillary holes exposed to a pulsed very high frequency plasma

Makoto Moriyama[1], Naoya Nakahara[1], Akihiro Mitsuya[1], Haruka Suzuki[1], Kazuaki Kurihara[3], Daiki Iino[3], Hiroyuki Fukumizu[3] and Hirotaka Toyoda[1,2]

[1]*Department of Electronics, Nagoya University, Furo-cho, Chikusa-ku, Nagoya 464-8603, Japan*
[2]*Center for Low-temperature Plasma Sciences, Nagoya University, Furo-cho, Chikusa-ku, Nagoya 464-8603, Japan*
[3]*Institute of Memory Technology Research & Development, Kioxia Corp. Isogo-ku Yokohama, 235-0017, Japan*

Abstract

Absolute values of the surface charge densities at the top and bottom of a capillary plate (CP) placed on a powered electrode were evaluated under the influence of pulse-modulated very high frequency (VHF, 40 MHz) plasma. The peak-to-peak voltage at the top and bottom of the CP was measured using a high-voltage probe; this voltage was carefully calibrated, removing the influence of probe impedance. Based on the peak-to-peak voltage, the capacitances of the sheath and the CP were evaluated. Based on the average voltage, the surface charge density was evaluated for the plasma-on and off phases. A charge density of the order of 10^{-5} C/m^2 was obtained at the bottom of the CP. Furthermore, two important observations were made during the plasma-off phase, namely: conservation of the surface charge density on the bottom of the CP and presence of the residual negative surface charge on the top of the CP.

Keywords:

high-aspect hole, charge-up, VHF plasma, charge density

1. Introduction

Anisotropic etching is an important process in nanoscale device fabrication. For achieving further device shrinkage, a precise etching process at the nanometer scale is required. It is well known that anisotropic etching utilizes neutral radical species and highly directional ions that are accelerated by the sheath in front of the substrate; this enhances the etching on the bottom surface, while suppressing it on the sidewall. As anisotropic etching is based on a critical balance of ion and neutral species, surface reaction processes are complex; this makes precise etching difficult. To achieve a precise etching performance, current technology utilizes dual-frequency plasma (DFP) sources wherein high-density plasma and high-bias voltage is realized by a combination of very high frequency (VHF) and low frequency (LF) power for producing the plasma and the bias voltage, respectively. This combination enables precise etching through an independent control of the plasma density and the ion impingement energy. Various studies of DFPs have been conducted from the perspective of theory, [1)] experiments, [2)] and simulations. [3,4)]

Apart from the studies on plasma sources, intensive research has also been carried out on the feature control of etching holes. [5-9)] For instance, bowing is a known issue in high aspect ratio (HAR) etching, wherein high energy ions are scattered on the tapering surface of the resist mask impinge on the sidewall of the etching hole to enhance localized sidewall etching. Charge-up of the etching holes or trenches also disturbs the precise control of the etching feature because the surface charge distorts the ion trajectory, reduces the etching rate and leads to feature degradation.

A better understanding of ion energy distribution (IED) in a substrate is important with regard to the charge-up origin of the etching holes or the trenches in the etching equipment. The IED is known to have a bi-modal profile[10)]. This has been experimentally studied using Faraday cup[11)] or quadrupole mass spectrometer with energy analyzer,[12,13)] and has also been analytically predicated[14)] and assessed using detailed simulation.[15)] The influence of the charge-up on the device damage has also been reported.[16,17)]

In the actual etching process, charge-up behavior has been found to depend on the etching material. For example, studies on the etching feature of conductive poly-Si at the edge of open and narrow patterns have shown pattern-dependent charge-up

behavior through experiments[18,19] and simulation[20-23]. Charge-up behavior in dielectric etching holes has been extensively studied, along with the influence of the charge build-up on etching rate[24]. Furthermore, the conductivity of fluorocarbon films on the sidewall of etching holes has also been studied.[25-27]

Several studies have proposed the suppression of charge-up by using neutral beam [28,29] and the charge-up behavior on the etching feature has been elucidated using simulation.[30,31] Charge cancellation in etching holes or trenches is required to minimize the deformation of the etching feature. For this purpose, the cancellation of accumulated charge using electron beam[32] or negative ions [33,34] has been considered. Among various techniques to suppress charge-up on the bottom surface of the hole, pulse-operation of plasma source[24, 35-37] is presently considered useful in practical etching processes. Moreover, considering the recent developments in high-density plasma sources, elucidation of a VHF plasma source with pulsed operation is potentially important for future high aspect ratio (HAR) etching processes.

Experimental studies on the charge-up behavior at the bottom of the etching hole have been conducted by several researchers. Kurihara et al. investigated fluorocarbon capacitively-coupled plasma at 13.56 MHz and measured fluorocarbon ions passing through the capillary plate. They tested a commercially-available plate having small HAR holes[12] and a specially-made capillary plate[38] using a mass spectrometer with an energy analyzer. Ohtake et al. reported voltage variation at the bottom of a specially-made capillary plate in a 13.56 MHz pulsed inductively-coupled plasma (ICP).[39] Negishi et al. used commercially available capillary plate (AR: <20) as a model of the etching hole and investigated the charge-up at the bottom of the microchannel-plate (MCP) in a 200 MHz electron cyclotron resonance (ECR) plasma.[40] These studies investigated the ion and charge-up behaviors on the bottom of the real-scale or real AR holes and provided important information on the performance of the HAR bottom in response to charge-up. However, to the best of our knowledge, no study has reported the absolute measurement of charge-density at the bottom and top of the HAR holes. Moreover, no study has yet described the variation in the charge densities at the top and bottom of a HAR hole in a pulse-operated plasma.

In this study, we elucidated the surface charge densities at the top and bottom of a capillary plate in a pulse-operated 40 MHz VHF capacitively-coupled plasma.

Capacitances of the sheath, capillary plate, and alumina insulator were experimentally evaluated from peak-to-peak voltage measurements at the top and bottom of the capillary plate and a powered electrode. Absolute charge densities were obtained from the average electrode voltages during plasma-on and -off conditions by using experimentally obtained capacitances. Although capillary plates were used for charge density evaluation of the HAR holes, the present study also describes a general model for assessing the absolute charge density of HAR holes that can predict the charge densities of actual HAR holes in the semiconductor device fabrication process. Moreover, the charge density of the contact hole is a vital parameter to assess temporal variation in the potentials of the HAR holes during the pulse-plasma operation and generates information on the optimization of the discharge operation recipe.

2. Experimental setup

For this study, a VHF plasma source was used (Fig. 1(a)). A vacuum vessel of diameter 16 cm and height 18 cm was evacuated by a turbo-molecular pump (nominal pumping speed: 200 l/s) at a base pressure of ~10^{-4} Pa. A powered electrode and a grounded electrode of equal diameter (11 cm) were placed at the bottom and top of the vessel, respectively, with electrode distance of 3 cm. The powered electrode was covered by an alumina plate (1.0 mm thick). Discharge gas (Ar) was introduced into the vessel from the grounded electrode through a mass flow controller at a rate of 30 sccm. Pressure was monitored by a capacitance manometer and was controlled by a conductance valve of the gas exhaust port at 2 Pa. CW or pulse-modulated 40 MHz VHF power (peak power <600 W, pulse frequency 1 kHz, pulse duty ratio 50%) was applied to the powered electrode through a matching box. Plasma parameters (density, electron temperature, and potential) were measured by a RF-compensated Langmuir probe (tip diameter 0.3 mm, tip length 5 mm), as shown in Fig. 1(b). In the Langmuir probe experiment, the fluctuation in the sheath voltage between the plasma and the probe tip is crucial for accurate measurement. To suppress the sheath voltage fluctuation in front of the probe, a LC tank circuit at a resonance frequency of 40 MHz was installed in the vicinity of the probe tip. A metal wire connected to the probe through a capacitor was wound to the insulating ceramic tube, which also helped the tip to follow the plasma potential

fluctuation. The probe was inserted from the sidewall of the vessel and was set at the center of the discharge region in both radial and axial directions.

We used capillary plates (CPs) as a model of the HAR hole and investigated electrical charge accumulated at both the top and the bottom of the CP. Three types of CP setups were used (Fig. 1(c)) using identical CPs (capillary diameter 25 mm, hole diameter 6 μm, plate thickness 0.3 mm, and aperture ratio 60%). We measured VHF peak-to-peak voltage (V_{PP}) and the average voltage (V_{AVE}), wherein the VHF oscillation component was removed. To correlate the V_{PP} with the V_{AVE} appearing at the top of the CP (self-bias voltage), we used the Type-1 setup wherein a metal electrode (of diameter equal to that of CP) was set at the top of the CP. Similarly, for evaluating V_{PP} and V_{AVE} appearing at the bottom of the hole, we used the Type-2 setup. The relationship of V_{PP} between the top and bottom of the CP was evaluated using the Type-3 setup wherein the metal electrodes were set both at the top and the bottom of the CP. Voltages were measured by high-voltage probes (HVPs) through a vacuum feedthrough at the top (Probe A) and the bottom (Probe B). Powered electrode voltage was measured using a separate HVP. Frequency characteristics of all HVPs were carefully calibrated taking the stray capacitance of the vacuum feedthrough into account. Flat frequency response characteristics from 1 kHz to 40 MHz were obtained using a 1 kHz pulse-modulated 40 MHz signal from a function generator.

3. Results and Discussions

3.1 Plasma parameters

The continuous wave (CW) VHF power dependences of plasma density n, electron temperature (T_e), and plasma potential (V_P) at an Ar pressure of 4.0 Pa are shown in Fig. 2. Plasma density monotonically increased with VHF power and was n~2×10^{17} m^{-3} at a VHF power of 300 W. Both electron temperature and plasma potential were almost constant (T_e~3.0 eV and V_P~26 V, respectively) with respect to VHF power. Plasma potential increased with reduction in pressure and V_P=31 V was obtained at an Ar pressure of 2.0 Pa.

3.2 Top and bottom voltages of the capillary plate

Figure 3 (a) and (b) show typical voltage waveforms at the top and bottom of the CP measured by Type-1 and Type-2 setups, respectively. VHF power, Ar pressure, pulse modulation frequency and duty ratio were 400 W, 2 Pa, 1 kHz and 50%, respectively. Amplitude of RF voltage (V_{PP}) was obtained by smoothing four consecutive data points of 40 MHz oscillation component using a peak detection function of the oscilloscope at sampling frequency 500MHz. V_{AVE} was calculated as mean value of the positive and negative peak voltages. During plasma-on condition the top voltage oscillated at V_{PP}~420 V for the CP top electrode (Fig. 3(a)) and V_{AVE} of ~190 V (self-bias voltage) was obtained. When the VHF pulse power was turned off both V_{PP} and V_{AVE} at the top immediately became 0 V. For the CP bottom electrode (Fig. 3(b)), V_{PP} was ~450 V, which was marginally higher than that for the top. Notably, V_{AVE} for the bottom electrode during the plasma-on condition was ~20 V, which was significantly different from that at the top electrode. Furthermore, V_{AVE} for the bottom electrode was ~150 V during the plasma-off period. This indicates that the bottom electrode was positively charged throughout the plasma-on and off periods by ions reaching the bottom of the CP. We observed a slight decay in the bottom voltage during the plasma-off period. Based on our time-resolved measurement of electron density using surface wave probe time decay constant of the electron density after turning off the VHF power was ~150 μs. This suggests that the slight decay in the bottom voltage during the plasma-off period (i.e., relaxation of the positive bottom charge) was related to the electrons coming from the afterglow plasma. The slight negative peak immediately after turning the plasma on was presumably induced by the re-charging of the bottom electrode to compensate the relaxed charge during the plasma-off period.

Next, we measured the voltages for the top and bottom electrodes, varying the pulsed VHF power. V_{PP} and V_{AVE} were calculated as a function of VHF power for both plasma-on and off periods. Hereafter, V_{PP} for top and bottom electrodes are indicated as V_{PP}^{TOP} and V_{PP}^{BTM}, respectively. Similarly, V_{AVE} for top and bottom electrodes (obtained by smoothing the 40 MHz component) are depicted as V_{AVE}^{TOP} and V_{AVE}^{BTM}, respectively. All voltages at plasma-on and off periods were measured at the last 1 μs of the VHF pulse-on and off periods, respectively (see Figs. 4(a) and (b)). Voltages at the CP top and bottom are measured using Type-1 and Type-2 setups, respectively. We

find that V_{PP}^{TOP} and V_{PP}^{BTM} monotonically increased with power. V_{AVE}^{TOP} monotonically decreased (negatively biased) with the VHF power when plasma was on and became almost 0 V when plasma was off. Compared to V_{AVE}^{TOP} the V_{AVE}^{BTM} was 0 to 20 V when plasma was on and increased up to ~180 V at a VHF power of 600 W when plasma was off.

It has been observed that the bottom of the hole tends to be positively charged compared to the top due to a difference in ion and electron flux. When plasma is on ions are accelerated by the sheath voltage and are injected into the hole at the CP bottom electrode. Electrons are also introduced into the hole at the moment when instantaneous CP top voltage reaches its maximum. However, angular distribution of the incident electrons is more widespread because of isotropic energy distribution due to thermal motion. Therefore, few electrons reach the CP bottom, which induces a difference in positive and negative flux at the CP bottom. Hence, response of V_{AVE}^{BTM} during plasma-on and off states can be explained as follows. The net positive current at the CP bottom causes increase in voltage with the VHF oscillation cycle. However, when the CP bottom voltage approaches the plasma potential the ions are decelerated by the voltage difference between the CP top and bottom, resulting in suppression of ion current at the CP bottom electrode. Concurrently, electrons are introduced into the hole at a moment when the instantaneous CP top voltage reaches its maximum, i.e., electron current flows on to the CP top surface to balance the surface charge and form the self-bias voltage.[21)] As the CP bottom voltage is always positive with respect to the top due to the positive CP bottom charge-up electrons are accelerated to reduce the positive charge-up at the CP bottom. In this situation the CP bottom electrode automatically acquires a voltage to balance positive and negative currents to attain the steady state CP bottom voltage. The result that V_{AVE}^{BTM} is close to the plasma potential during the plasma-on condition indicates that the ion kinetic energy plays an important in balancing the positive and negative currents in the hole.

V_{AVE}^{BTM} increased up to ~170 V at a peak VHF power of 600 W when the plasma was turned off (Fig. 4(b)). This does not necessarily indicate a change in surface charge at the CP bottom, because changes in V_{AVE}^{TOP} can influence the V_{AVE}^{BTM}. Detailed investigation can measure absolute surface charge densities of the CP top and bottom (discussed later).

3.3 Evaluation of top surface voltage of the CP without HVP

The above results were obtained using HVP with vacuum feedthrough for voltage monitoring. In VHF, however, slight stray capacitances may influence measurements and the data must be analyzed carefully. For example, the top surface peak-to-peak voltages V_{PP}^{TOP} measured by the Type-1 and Type-2 CPs do not precisely correspond because Type-2 CP does not have the electrode and the HVP. The same problem also occurs for V_{AVE} measurement, as the V_{AVE} of the top surface is determined by the V_{PP} appearing on the top surface of the CP.

To resolve this issue an equivalent circuit model was applied to estimate the top voltages V_{PP} and V_{AVE} without the HVP and the electrode (see Fig. 5 for details). Here, C_{ALM} indicates the capacitance between the powered electrode and the bottom electrode of the CP; C_{CP} indicates the effective capacitance between the top and the bottom electrodes of the CP considering the hole space in it; C_{FT} indicates feedthrough stray capacitance between two wires that are connected to the top and bottom CP electrodes; C_S is effective sheath capacitance between the plasma and the top electrode and is considered as a function of the VHF power. C_A, C_B and R_A, R_B are input capacitances (3 pF) and input resistances (100 MΩ), respectively, of two identical HVPs used for the top and bottom CP electrode measurements. In the present study impedances of C_A and C_B were considerably smaller than those of R_A and R_B and input resistances in the model were considered negligible. Circuits with and without the jumper wires represent Type-3 and Type-2 setups, respectively. Resistance across the CP top and bottom was neglected in the model because it is much larger than the capacitive reactance across the CP top and bottom. In actual fluorocarbon plasma etching, however, the fluorocarbon polymer film acts as a current path through the hole. In the case of the fluorocarbon plasma additional resistance across the CP top and bottom should be considered in the model.

Capacitances C_{FT} and C_{ALM} were measured as 5.8 pF and 22 pF, respectively, using an impedance meter. Based on the equivalent circuit model capacitances C_{CP} and C_S were evaluated from V_{PP} measurement using the Type-3 setup during the VHF discharge (Fig. 6(a)). V_{PP} monotonically increased with VHF power and the V_{PP}^{ELEC} was almost double of V_{PP}^{BTM} or V_{PP}^{TOP}. V_{PP}^{TOP} was slightly smaller than the V_{PP}^{BTM} (c.f.

Fig. 4). This suggests that the impedance across the CP was smaller than those across the alumina plate or the sheath, although the influence of stray capacitances needs to be examined. The V_{PP} ratios $R_{BE}=V_{PP}^{BTM}/V_{PP}^{ELEC}$ and $R_{TB}=V_{PP}^{TOP}/V_{PP}^{BTM}$ were ~0.58 and ~0.87, respectively, showing very weak dependences on the VHF power (Fig. 6(b)). From these we estimated capillary capacitance C_{CP} and the effective sheath capacitance C_S (Fig. 6(c)). C_{CP} was almost constant at 48 pF, while C_S marginally increased up to ~2 pF with VHF power. This increase in C_S can be explained by the decrease in the sheath thickness with VHF power. Sheath thickness can be approximated from the ion flux and sheath voltage using the Child-Langmuir sheath model (sheath voltage >> electron temperature). Using the measured voltage and the ion flux evaluated from the plasma density a sheath thickness of 1.4 mm was obtained at V_{PP}^{TOP} of 900 V, and resultant effective sheath capacitance was ~2 pF, which is fairly consistent with results obtained from the equivalent circuit model.

As the HVP is not connected to the top of the CP in the Type-2 setup the only way to estimate V_{PP}^{TOP} is from the equivalent circuit parameters after removing C_A and C_{FT} from the circuit. Hereafter, this estimated V_{PP}^{TOP} is indicated as $V_{PP}^{TOP\_EST}$. The ratio of the $V_{PP}^{TOP\_EST}$ to the V_{PP}^{BTM} is termed as R_{TB}^{EST} that can be obtained from the relation: $R_{TB}^{EST}=V_{PP}^{TOP\_EST}/V_{PP}^{BTM}=C_{CP}/(C_{CP}+C_S)$. The calculated R_{TB}^{EST} was larger than the R_{TB}, demonstrating the importance of stray capacitance evaluation for the VHF peak-to-peak voltage measurement (Fig. 6(b)). From the measured V_{PP}^{BTM} and R_{TB}^{EST} the $V_{PP}^{TOP\_EST}$ for Type-2 setup was evaluated (Fig. 4(a)), which was slightly higher than V_{PP}^{TOP} measured by the Type-1 setup. We then estimated the average top voltage without the HVP ($V_{AVE}^{TOP\_EST}$) from $V_{PP}^{TOP\_EST}$ in the Type-2 setup (note that Fig. 7 shows V_{AVE}^{TOP} as a function of V_{PP}^{TOP} measured by the Type-1 setup). V_{AVE}^{TOP} decreased almost linearly with V_{PP}^{TOP} as expected from the theory of RF self-bias. As $V_{AVE}^{TOP\_EST}$ in the Type-2 setup was supposed to follow this relationship (shown in Fig. 7) $V_{AVE}^{TOP\_EST}$ was estimated from $V_{PP}^{TOP\_EST}$. We assessed VHF power dependence of the $V_{AVE}^{TOP\_EST}$ during plasma-on phase using the Type-2 setup (Fig. 4(b)). Although the difference between V_{AVE}^{TOP} in Type-1 and $V_{AVE}^{TOP\_EST}$ in Type-2 was coincidentally small the accurate results should be obtained from $V_{AVE}^{TOP\_EST}$ because a small difference is not always the case.

3.4 Surface charge density evaluation

From V_{AVE} and capacitances derived from the equivalent circuit model above we estimated charge densities at the top and bottom of the CP using the electrostatic model described in Fig. 8. In the actual structure, sheath charge spreads in the sheath region. In this model, however, the charge is considered as a surface charge density placed at the plasma-sheath boundary. When a sheet charge σ exists in a space electric flux density $D=\sigma/2$ is induced normal to the sheet surface. Hence, electric flux densities induced by the sheath surface charge σ_P, the CP top surface charge σ_T, the CP bottom surface charge σ_B and the powered electrode surface charge σ_E are expressed as:

$$D_P = \sigma_P/2,\ D_T = \sigma_T/2,\ D_B = \sigma_B/2,\ D_E = \sigma_E/2 \quad (1)$$

From the principle of superposition the flux density at the sheath D_S, capillary plate D_{CP} and alumina plate D_{ALM} are expressed as:

$$D_S = D_P - D_T - D_B - D_E, \quad (2)$$

$$D_{CP} = D_P + D_T - D_B - D_E, \quad (3)$$

$$D_{ALM} = D_P + D_T + D_B - D_E, \quad (4)$$

As the electric fields in the metal electrode and the plasma are almost zero we also obtain the following equation:

$$D_P + D_T + D_B + D_E = 0 \quad (5)$$

Using electric flux densities voltages across the sheath (V_S), capillary plate (V_{CP}) and the alumina plate (V_{ALM}) are obtained as:

$$V_S = E_S d_S = -D_S(d_S/\varepsilon_o) = -D_S/C_S, \quad (6)$$

$$V_{CP} = E_{CP} d_{CP} = -D_{CP}(d_{CP}/\varepsilon_o\varepsilon_{CP}) = -D_{CP}/C_{CP}, \quad (7)$$

$$V_{ALM} = E_{ALM} d_{ALM} = -D_{ALM}(d_{ALM}/\varepsilon_o\varepsilon_{ALM}) = -D_{ALM}/C_{ALM}. \quad (8)$$

Surface charge densities σ_S, σ_T, σ_B and σ_E were obtained by solving eqs. (6)-(8) using eqs. (1)-(5) as a function of the $V_{AVE}^{TOP\_EST}$ (Fig. 9). Positive surface charge accumulation and its increase with the $V_{AVE}^{TOP\_EST}$ was observed at the bottom electrode of the CP (Fig. 9(c)). The charge density at the bottom of the CP during plasma-off condition was lower than during plasma-on. Voltages at both plasma-on and off phases reached their steady states (Fig. 2), although slight voltage variations were observed immediately after turning the plasma on or off. This indicates that the positive charge at the bottom of the CP leaked during plasma-off and accumulated during plasma-on condition. Charge accumulation at the top of the CP during plasma-on was not observed at that time scale because the charge-up rate is higher at the top of the CP than at the bottom. Charge density at the sheath was considerably lower than that of the capillary plate because the equivalent sheath capacitance was smaller than other capacitances (Fig 9(a)). Negative surface charge density monotonically increased with V_{AVE}^{TOP} during plasma-on condition (Fig. 9(b)). Notably, the surface charge at the CP top was not zero even during the plasma-off period. This was because some negative charge must remain on the surface to shield the electric field induced by the accumulated positive charge at the CP bottom. The situation was similar at the powered electrode (Fig. 9(d)) and negative surface charge existed during the plasma-off phase.

The present study demonstrates the estimation of absolute charge density at the CP bottom, wherein V_{PP} and V_{AVE} measurements were used for modeling of the equivalent circuit and evaluation of charge density, respectively. If ion and electron fluxes during the plasma-on and off periods are evaluated it is possible to derive the time scales of charge up and charge relaxation, respectively. These time scales are important parameters to optimize operation protocols for the pulse plasma discharge. Although the present study did not reproduce the actual etching process, the models described herein can be used to estimate the absolute charge density at the bottom of actual etching holes and will contribute to the improvement of the process protocols.

4. Conclusion

In this study, the charge-up behavior of a CP in a pulse-modulated 40 MHz capacitively-coupled Ar plasma was studied. Furthermore, the surface charges

accumulated at the top and bottom surfaces of the CP were evaluated. Three types of CP setups with different electrode combination were used and the VHF peak-to-peak voltages (V_{PP}) and average voltages (V_{AVE}) were measured during the pulse-operated VHF discharge. The influence of the probe impedance on the V_{PP} and V_{AVE} measurements was investigated and accurate voltages on the top of the CP were estimated from an equivalent circuit model. In this model, circuit parameters such as CP capacitance and sheath capacitance were evaluated experimentally. From the measured V_{AVE} and evaluated capacitances, surface charge densities on the top and bottom of the CP were obtained. Surface charge density of the CP bottom was partly reduced through a high-voltage probe during the plasma-off period and was observed to accumulate a positive charge during the plasma-on period. Residual charge at the CP top surface was also observed during the plasma-off period. These results suggest that the charge accumulation will be higher during the actual scale etching.

References

1) M. M. Turner and P. Chabert: Phys. Rev. Lett. **96** (2006) 205001.
2) J. Schulze, T. Gans, D. O'Connell, U. Czarnetzki, A. R. Ellingboe and M. M. Turner: J. Phys. D. Appl. Phys. **40** (2007) 7008.
3) T. Shimada, T. Yagisawa and T. Makabe: Jap. J. Appl. Phys. **45** (2006) 8876.
4) T. Makabe and T. Yagisawa: Plasma Sources Sci. Technol.**18** (2009) 014016.
5) H. Jansen, H. Gardeniers, M. De Boer, M. Elwenspoek and J. Fluitman: J. Micromech. Microeng. **6** (1996) 14.
6) H. Abe, M. Yoneda and N. Fujiwara: Jpn. J. Appl. Phys. **47** (2008) 1435.
7) B. Wu, A. Kumar and S. Pamarthy: J. Appl. Phys.**108** (2010) 051101.
8) T. Iwase, Y. Kamaji, S. Y. Kang, K. Koga, N. Kuboi, M. Nakamura, N. Negishi, T. Nozaki, S. Nunomura, D. Ogawa, M. Omura, T. Shimizu, K. Shinoda, Y. Sonoda, H. Suzuki, K. Takahashi, T. Tsutsumi, K. Yoshikawa, T. Ishijima and K. Ishikawa: Jpn. J. Appl. Phys. **58** (2019) SE0802.
9) J. P. Gambino, S. A. Adderly and J. U. Knickerbocker: Microelectron. Eng. **135** (2015) 73.
10) E. Kawamura, V. Vahedi, M. A. Lieberman and C. K. Birdsall: Plasma Sources Sci. Technol. **8** (1999) R45.

11) A. Manenschijn, G. C. A. M. Janssen, E. Van Der Drift and S. Radelaar: J. Appl. Phys. **69** (1991) 1253.
12) K. Kurihara and M. Sekine: Plasma Sources Sci. Technol. **5** (1996) 121.
13) Z. C. Li, D. L. Chang, X. S. Li, Z. H. Bi, W. Q. Lu, Y. Xu, A. M. Zhu and Y. N. Wang: Phys. Plasmas **17** (2010) 033501.
14) P. Benoit-Cattin and L. C. Bernard: J. Appl. Phys. **39** (1968) 5723.
15) V. Georgieva, A. Bogaerts and R. Gijbels: Phys. Rev. **69** (2004) 026406.
16) W. M. Greene, J. B. Kruger and G. Kooi: J. Vac. Sci. Technol. **9** (1991) 366.
17) K. Hashimoto: Jpn. J. Appl. Phys. **33** (1994) 6013.
18) N. Fujiwara, T. Maruyama and M. Yoneda: Jap. J. Appl. Phys. **34** (1995) 2095.
19) N. Fujiwara, T. Maruyama and M. Yoneda: Jpn. J. Appl. Phys. **35** (1996) 2450.
20) T. Kinoshita, M. Hane and J. P. McVittie: J. Vac. Sci. Technol. **14** (1996) 560.
21) G. S. Hwang and K. P. Giapis: J. Appl. Phys. **81** (1997) 3433.
22) G. S. Hwang and K. P. Giapis: J. Vac. Sci. Technol. **15** (1997) 1741.
23) V. Ishchuk, B. E. Volland, M. Hauguth, M. Cooke and I. W. Rangelow: J. Appl. Phys. **112** (2012) 084308.
24) K. Yonekura, M. Kiritani, S. Sakamori, T. Yokoi, N. Fujiwara and H. Miyatake: Jap. J. Appl. Phys. **37** (1998) 2314.
25) T. Shimmura, S. Soda, S. Samukawa, M. Koyanagi and K. Hane: J. Vac. Sci. Technol. **22** (2004) 533.
26) T. Shimmura, S. Soda, S. Samukawa, M. Koyanagi and K. Hane: J. Vac. Sci. Technol. **20** (2002) 2346.
27) T. Shimmura, Y. Suzuki, S. Soda, S. Samukawa, M. Koyanagi and K. Hane: J. Vac. Sci. Technol. **22** (2004) 433.
28) S. J. Kim, H. J. Lee, G. Y. Yeom and J. L. Koo: Jap. J. Appl. Phys. **43** (2004) 7261.
29) S. Samukawa: Jap. J. Appl. Phys. **45** (2006) 2395.
30) J. C. Arnold and H. H. Sawin: J. Appl. Phys. **70** (1991) 5314.
31) A. P. Mahorowala and H. H. Sawin: J. Vac. Sci. Technol. **20** (2002) 1084.
32) M. Watanabe, D. M. Shaw and G. J. Collins: Appl. Phys. Lett. **79** (2001) 2698.
33) T. Shibayama, H. Shindo and Y. Horiike: Plasma Sources Sci. Technol. **5** (1996) 254.
34) H. Ohtake and S. Samukawa: J. Vac. Sci. Technol. **20** (2002) 1026.
35) S. Samukawa, and T. Mieno: Plasma Sources Sci. Technol. **5** (1996) 132.

36) C. J. Choi, O. S. Kwon and Y. S. Seol: Jpn. J. Appl. Phys. **37** (1998) 6894.
37) J. H. Kim, C. J. Kang, T. H. Ahn and J. T. Moon: Thin Solid Films **345** (1999) 124.
38) K. Kurihara and M. Sekine: Jpn. J. Appl. Phys. **39** (2000) 1369.
39) H. Ohtake, B. Jinnai, Y. Suzuki, S. Soda, T. Shimmura and S. Samukawa: J. Vac. Sci. Technol. **24** (2006) 2172.
40) N. Negishi, M. Miyake, K. Yokogawa, M. Oyama, T. Kanekiyo and M. Izawa, J. Vac. Sci. Technol. **35** (2017) 051205.

Figure captions

Fig. 1. (a) Experimental apparatus. (b) RF-compensated Langmuir probe. (c) Three types of capillary plate setups.

Fig. 2. VHF power dependences of (a) plasma density, (b) electron temperature and (c) plasma potential. Ar pressure is 2 Pa.

Fig. 3. Voltage waveforms of (a) CP top electrode in type-1 setup. (b) CP bottom electrode in Type-2 setup. VHF power is 400 W.

Fig. 4. (a) Peak-to-peak voltages of top electrode (V_{PP}^{TOP}) in Type-1 setup (filled circles) and bottom electrode (V_{PP}^{BTM}) in Type-2 setup (filled diamonds) as a function of VHF power. Estimated peak-to-peak voltage of CP top ($V_{PP}^{TOP\_EST}$) in Type-2 setup (open circles) is also indicated. (b) Average voltages of top electrode (V_{AVE}^{TOP}) in Type-1 setup (diamonds) and bottom electrode (V_{AVE}^{BTM}) in Type-2 setup (circles) as a function of VHF power. Estimated average voltage of CP top ($V_{AVE}^{TOP\_EST}$) in Type-2 setup (circles) is also indicated. Filled and open plots indicate plasma-on and off conditions, respectively.

Fig. 5. Equivalent circuit model of plasma, CP and powered electrode, including high-voltage probes and vacuum feedthrough.

Fig 6. (a) Peak-to-peak voltages of top electrode (V_{PP}^{TOP}), bottom electrode (V_{PP}^{BTM}) and powered electrode (V_{PP}^{ELEC}) as a function of VHF power using Type-3 setup. (b) V_{PP} ratios $R_{BE}(=V_{PP}^{BTM}/V_{PP}^{ELEC})$ and $R_{TB}(=V_{PP}^{TOP}/V_{PP}^{BTM})$ as a function of V_{PP}^{ELEC}. Estimated voltage ratio without HVP in Type-2 setup ($V_{PP}^{TOP\_EST}/V_{PP}^{BTM}$) is also indicated by open squares. (c) Sheath and CP capacitances evaluated from voltage ratios R_{BE} and R_{TB} using the equivalent circuit model.

Fig. 7. Average top CP voltage (V_{AVE}^{TOP}) as a function of the peak-to-peak top voltage (V_{PP}^{TOP}) using Type-1 setup.

Fig. 8. Electric field, electric flux density and surface charge in the vicinity of the CP.

Fig. 9. Surface charge densities of (a) sheath, (b) CP top, (c) CP bottom and (d) powered electrode, as a function of V_{AVE}^{TOP}. Filled and open circles indicate surface charges at plasma-on and off, respectively.

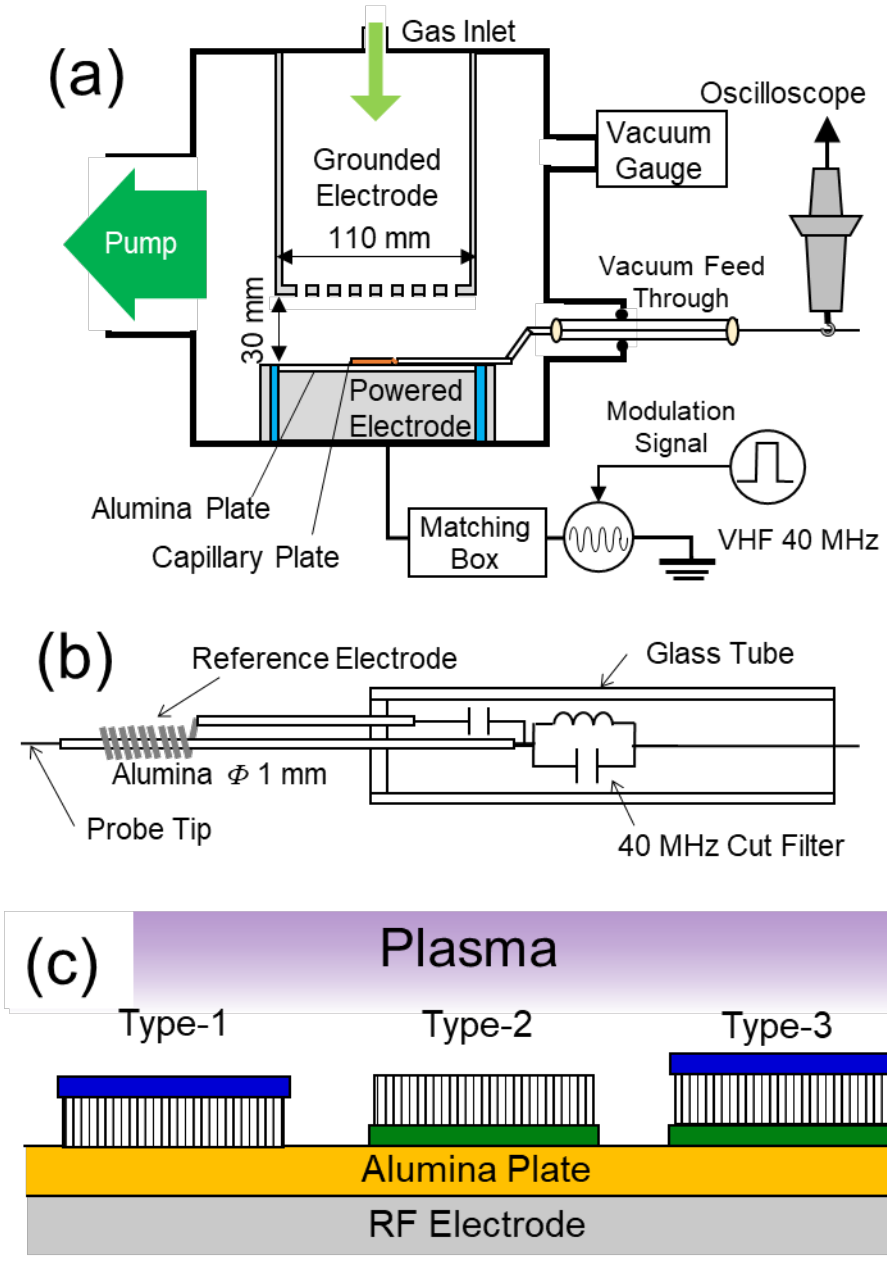

Fig. 1. (a) Experimental apparatus. (b) RF-compensated Langmuir probe. (c) Three types of capillary plate setups.

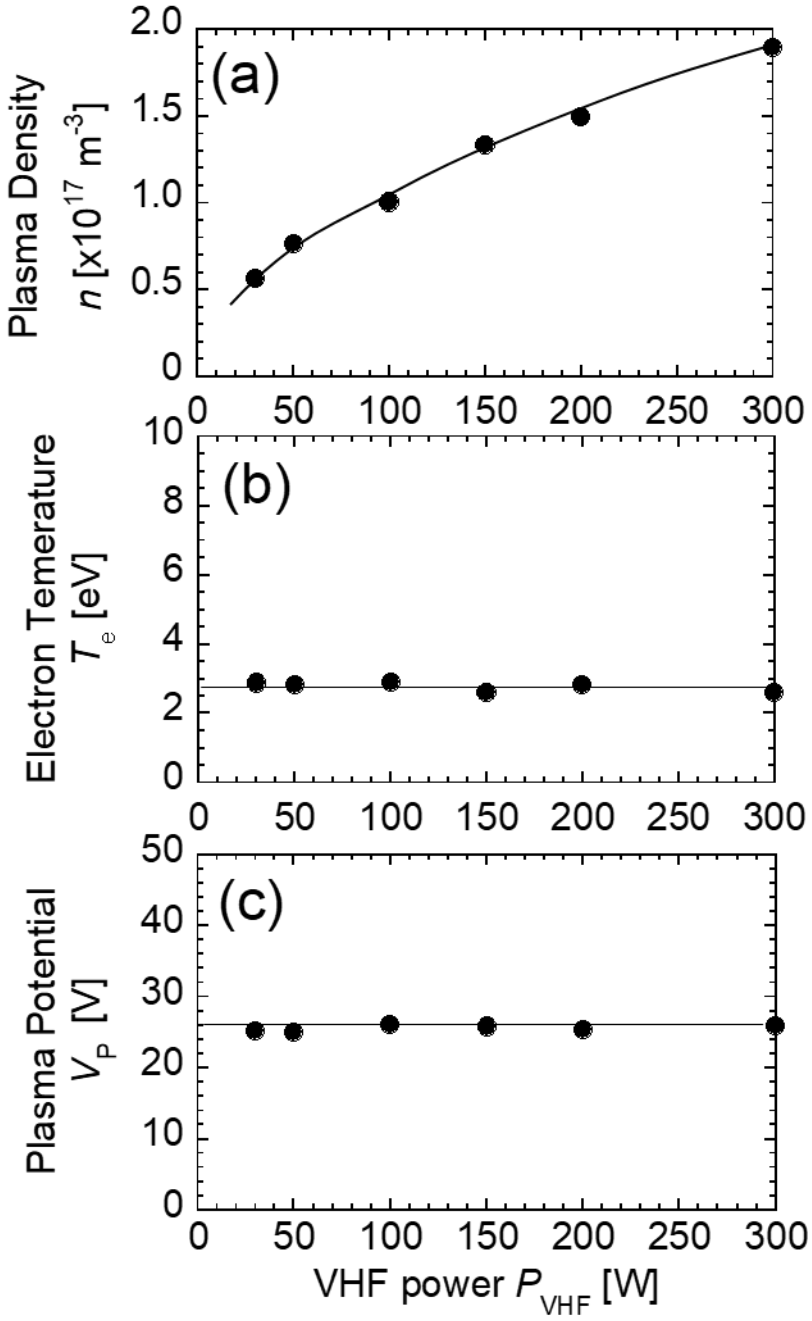

Fig. 2. VHF power dependences of (a) plasma density, (b) electron temperature and (c) plasma potential. Ar pressure is 2 Pa.

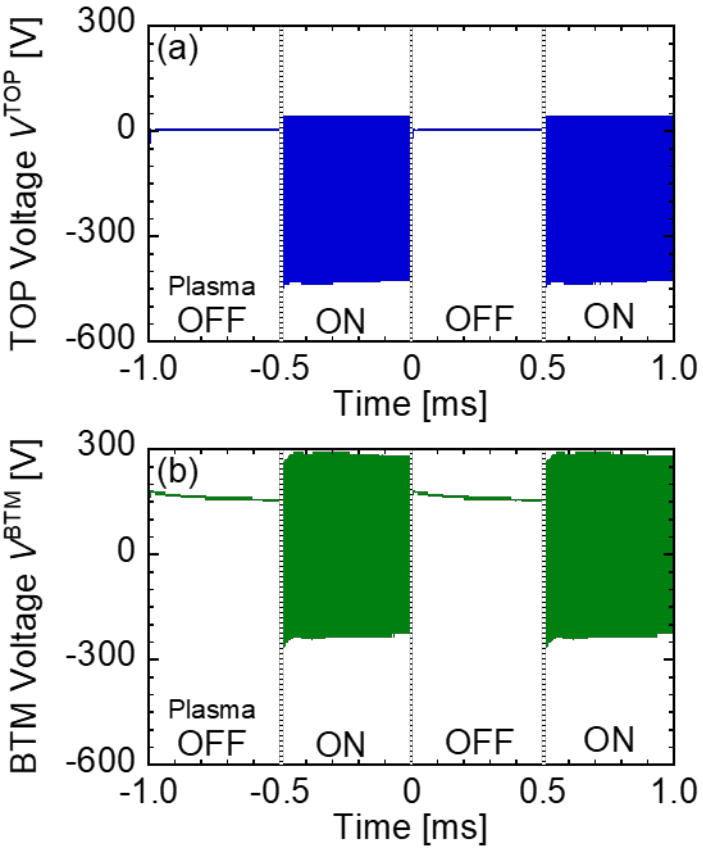

Fig. 3. Voltage waveforms of (a) CP top electrode in Type-1 setup. (b) CP bottom electrode in Type-2 setup. VHF power is 400 W.

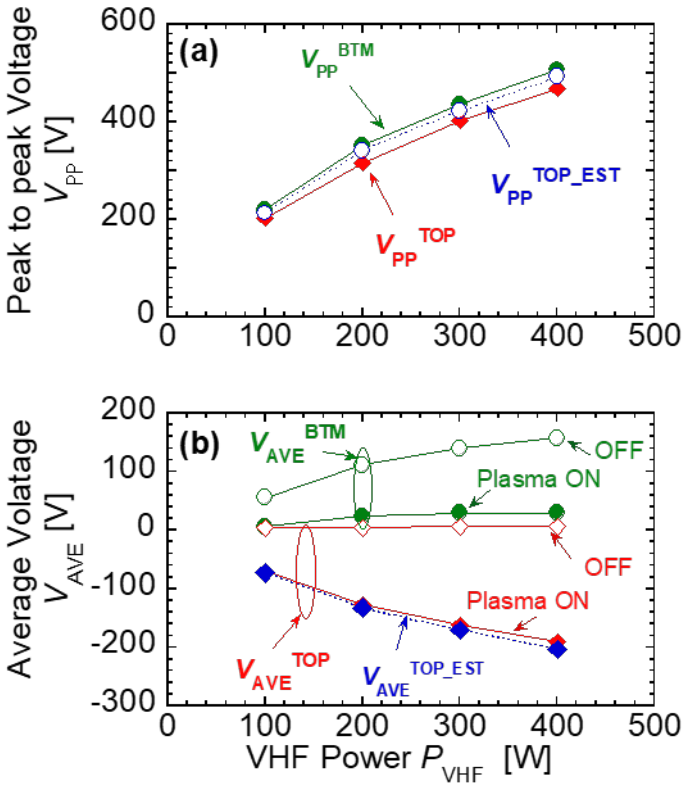

Fig. 4. (a) Peak-to-peak voltages of top electrode (V_{PP}^{TOP}) in Type-1 setup (filled diamonds) and bottom electrode (V_{PP}^{BTM}) in Type-2 setup (filled circles) as a function of VHF power. Estimated peak-to-peak voltage of CP top ($V_{PP}^{TOP\_EST}$) in Type-2 setup (open circles) is also indicated. (b) Average voltages of top electrode (V_{AVE}^{TOP}) in Type-1 setup (diamonds) and bottom electrode (V_{AVE}^{BTM}) in Type-2 setup (circles) as a function of the VHF power. Estimated average voltage of top ($V_{AVE}^{TOP\_EST}$) in Type-2 setup (circles) is also indicated. Filled and open plots indicate plasma-on and off conditions, respectively.

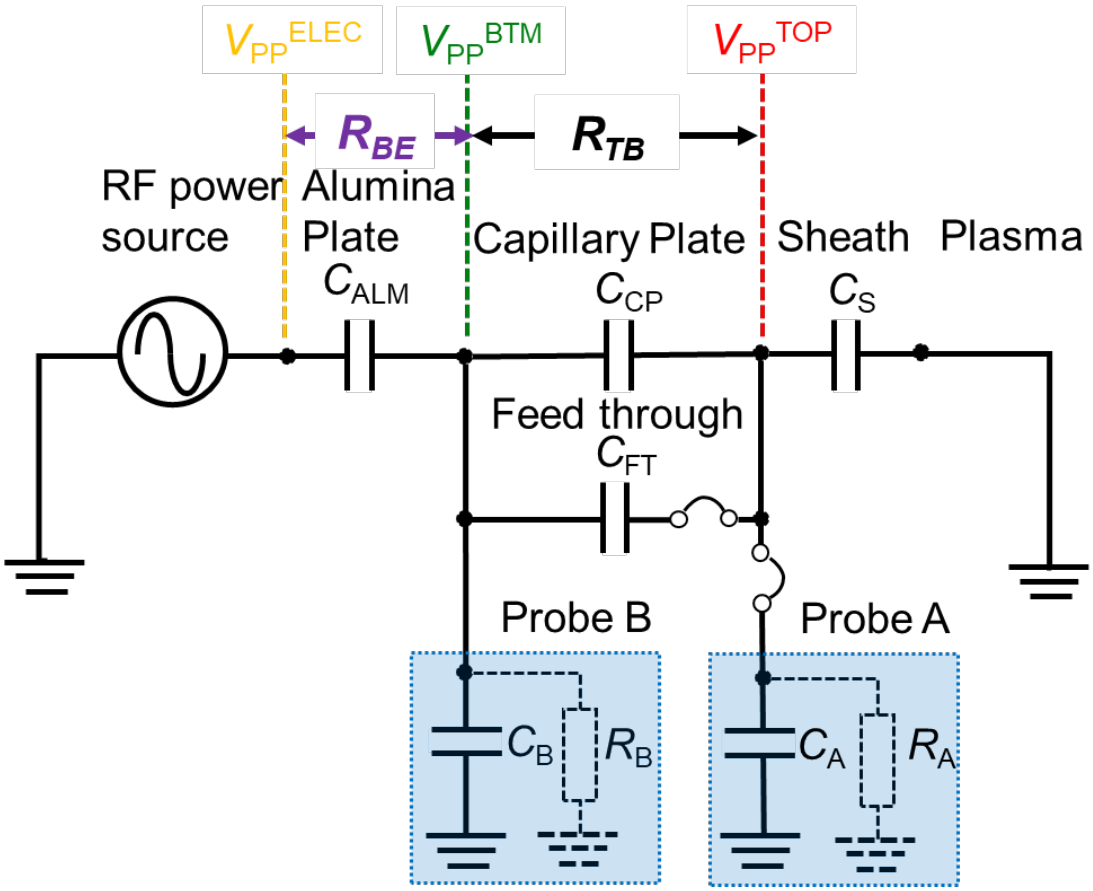

Fig. 5. Equivalent circuit model of plasma, CP and powered electrode, including high voltage probes and vacuum feedthrough.

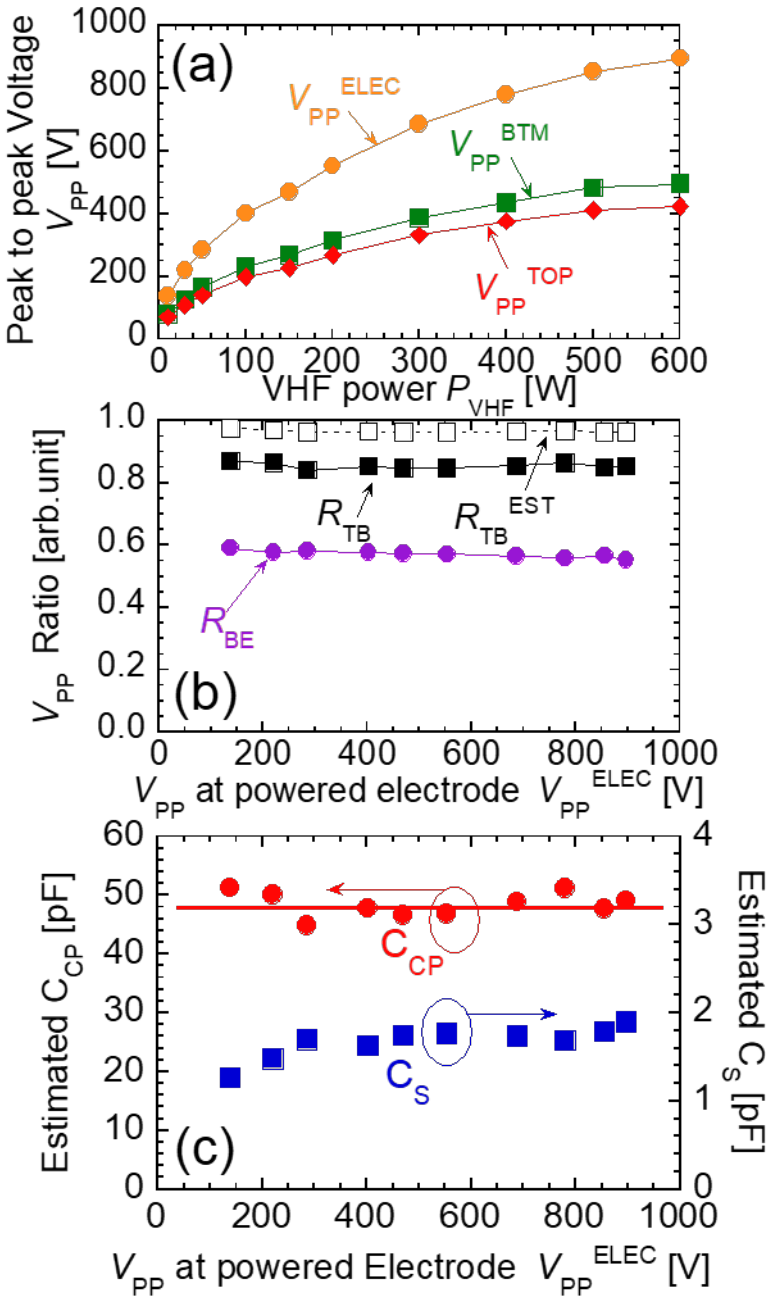

Fig 6. (a) Peak-to-peak voltages of top electrode (V_{PP}^{TOP}), bottom electrode (V_{PP}^{BTM}) and powered electrode (V_{PP}^{ELEC}) as a function of VHF power using Type-3 setup. (b) V_{PP} ratios R_{BE}(=$V_{PP}^{BTM}/V_{PP}^{ELEC}$) and R_{TB}(=$V_{PP}^{TOP}/V_{PP}^{BTM}$) as a function of V_{PP}^{ELEC}. Estimated voltage ratio without HVP in Type-2 setup ($V_{PP}^{TOP\_EST}/V_{PP}^{BTM}$) is also indicated by open squares. (c) Sheath and CP capacitances evaluated from voltage ratios R_{BE} and R_{TB} using the equivalent circuit model.

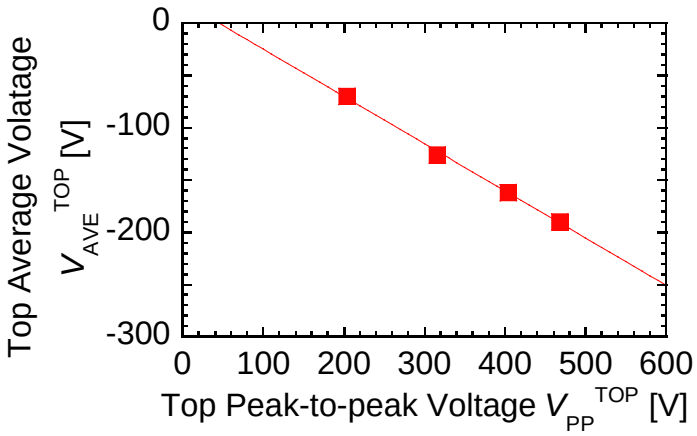

Fig. 7. Average top CP voltage (V_{AVE}^{TOP}) as a function of the peak-to-peak top voltage (V_{PP}^{TOP}) using Type-1 setup.

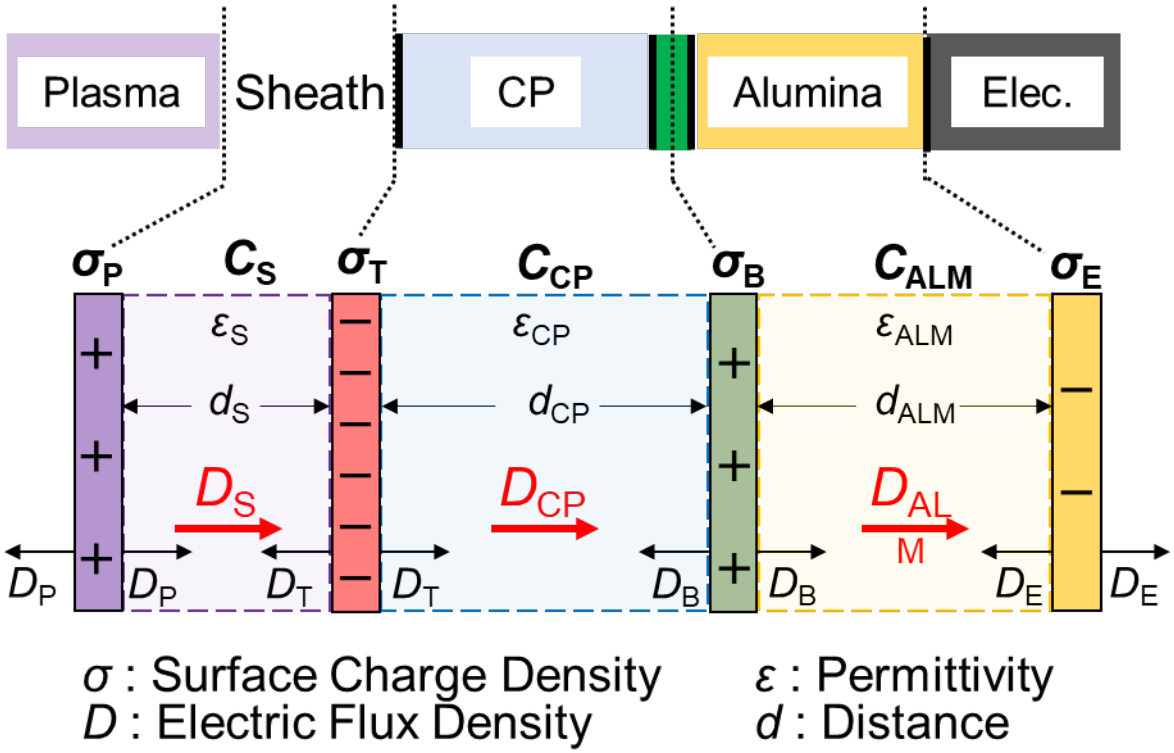

Fig. 8. Electric field, electric flux density and surface charge in the vicinity of the CP.

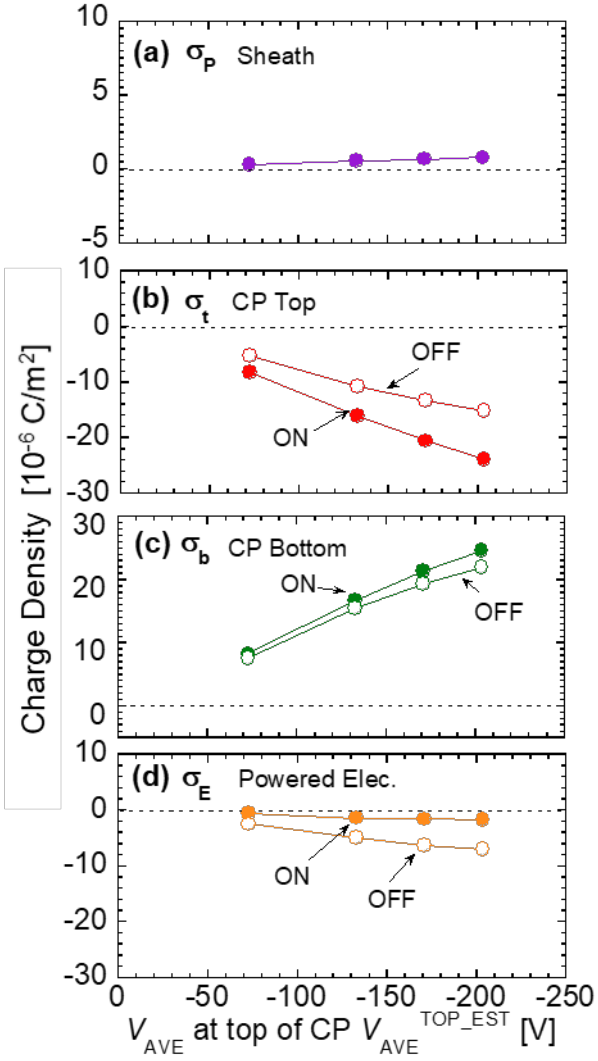

Fig. 9. Surface charge densities of (a) sheath, (b) CP top, (c) CP bottom and (d) powered electrode, as a function of the V_{AVE}^{TOP}. Filled and open circles indicate surface charges at plasma-on and off, respectively.